Integrative Biology

Accepted Manuscript

ROYAL SOCIETY OF CHEMISTRY

www.rsc.org/ibiology

Insight, innovation, integration

In many tumour cases, a need for more accurate delineation of tumour infiltration area in a patient-specific manner has arisen. The objective of this study was to build a mathematical model able to describe the growth and the real invasion pattern of multicellular tumour spheroids immersed in a collagen matrix. The model may be used in a descriptive (case-specific) as well as in a predictive (population-dependent) way, depending on the type of the input parameters (a shape function obtained from a given experimental case or an aleatory shape function generated by data mining and Monte Carlo tools from the entire dataset, respectively). This kind of empirical-numerical interaction has wide application potential at the basic research and at the clinical level.

Journal Name

ARTICLE TYPE

Cite this: DOI: 10.1039/xxxxxxxxxx

Mathematical modelling of microtumour infiltration based on *in vitro* experiments

Emmanuel Luján,[a] Liliana N. Guerra,[b] Alejandro Soba,[c] Nicolás Visacovsky,[a] Daniel Gandía,[d] Juan C. Calvo,[b] and Cecilia Suárez *[a]

Received Date
Accepted Date

DOI: 10.1039/xxxxxxxxxx

www.rsc.org/journalname

Present mathematical models of microtumours consider, in general, volumetric growth and spherical tumour invasion shapes. Nevertheless in many cases, such as in gliomas, a need for more accurate delineation of tumour infiltration areas in a patient-specific manner has arisen. The objective of this study was to build a mathematical model able to describe in a case-specific way as well as to predict in a probabilistic way the growth and the real invasion pattern of multicellular tumour spheroids (in vitro model of an avascular microtumour) immersed in a collagen matrix. The two-dimensional theoretical model was represented by a reaction-convection-diffusion equation that considers logistic proliferation, volumetric growth, a rim with proliferative cells at the tumour surface and invasion with diffusive and convective components. Population parameter values of the model were extracted from the experimental dataset and a shape function that describes the invasion area was derived from each experimental case by image processing. New possible and aleatory shape functions were generated by data mining and Monte Carlo tools by means of a satellite EGARCH model that were feed with all the shape functions of the dataset. Then the main model is used in two different ways: to reproduce the growth and invasion of a given experimental tumour in a case-specific manner when feed with the correspondent shape function (descriptive simulations) or to generate new possible tumour cases that respond to the general population pattern when feed with an aleatory-generated shape function (predictive simulations). Both types of simulations are in good agreement with empirical data, as it was revealed by area quantification and a Bland-Altman analysis. This kind of experimental-numerical interaction has wide application potential at the moment of designing new strategies able to predict as much as possible the invasive behaviour of a tumour in base on its particular characteristics and microenvironment.

1 Introduction

Computational oncology is a generic term that encompasses any form of computer-based modelling relating to tumour biology and cancer therapy[1,2]. The recent expansion of quantitative models in cancer research addresses many questions regarding tumour initiation, progression and metastasis as well as intratumour heterogeneity, treatment responses and resistance[3]. Latest mathematical models of tumour growth tends to be multiscaled and patient-specific[4]. Also, relatively simple models based on reaction-diffusion equations describing tumour proliferation and invasion into peripheral host tissue have proved to be of clinical relevance[5]. In a recent work we have developed a model of this kind to describe a human glioma growth in a patient-specific way[6]. There are also many mathematical approaches tending to predict the growth and invasion of avascular microtumours made in vitro, as is the case of multicellular tumour spheroids. Last approaches of this kind apply continuum, discrete or hybrid techniques[7].

Multicellular tumour spheroids provide a physiologically useful tool for cancer-related studies concerning tumourigenicity, drug delivery and therapeutic resistance, among others[8–10]. A derivation of this in vitro model consists on spheroids immersed in a three-dimensional matrix of gel where the microtumour is able to invade, being this one of the most evolved experimental models to study key aspects of tumourigenesis, like tumour migration and invasion in response to environmental factors[11,12]. The re-creation of the tumour microenvironment including a three-

[a] *Laboratorio de Sistemas Complejos, Departamento de Computación / Instituto de Física del Plasma, Facultad de Ciencias Exactas y Naturales, Universidad de Buenos Aires, CONICET, Buenos Aires, Argentina.*
[b] *Departamento de Química Biológica, Facultad de Ciencias Exactas y Naturales, Universidad de Buenos Aires, CONICET, Buenos Aires, Argentina.*
[c] *Centro de Simulación Computacional para Aplicaciones Tecnológicas, CONICET, Buenos Aires, Argentina*
[d] *Sanatorio Los Arcos, Buenos Aires, Argentina*
* *Corresponding author. E-mail: csuarez@dc.uba.ar*

dimensional structure with tumour-stroma interactions, cell-cell adhesion and cellular signaling is essential for a deeper understanding of the invasion process.

Loessner et al.[13] presented a mathematical model that describes the growth of multicellular tumour spheroids from human epithelial ovarian carcinoma in a bioengineered three-dimensional microenvironment. Stein et al.[14] presented a quasi-three-dimensional model based on a reaction-diffusion-convection equation to describe the growth and invasion of multicellular tumour spheroids from a glioblastoma cell line assuming spherical symmetry. This group also proposed an heuristic algorithm to estimate automatically the invasion radius in base on local fluctuations of the image intensity[15]. Taking aside some specific cases (see for example[16,17]) models related to avascular microtumours have in general centered in the description of the volumetric growth of the tumour core and of spherical tumour invasion areas. Nevertheless it is necessary at present to develop new strategies to better determine tumour infiltration borders as well as to predict as much as possible tumour spread characteristics in order to optimize treatments such as surgery or radiotherapy.

Here we present a two-dimensional mathematical model able to describe the growth and real invasion shape of individual multicellular tumour spheroids (descriptive simulations) as well as to generate new possible tumour cases that respond to the same population pattern in this specific environment (predictive simulations). This kind of theoretical/experimental framework has wide application potential both at the basic research and at the clinical level.

2 Methods

2.1 In vitro model

Multicellular tumour spheroids of the LM3 cell line (mouse epithelial and metastatic mammary tumour cells[18]), were generated by the hanging drop method[19]. This technique has the advantage of producing homogeneous spheroids and consists on seeding drops of 20 μl with 1500 cells each in the inner surface of a Petri dish cap. Once seeded, phosphate buffer solution was placed in the dish to maintain humidity and the cap returns to their natural position over the dish. After four days in culture at $37^{\circ}C$ and 5% CO_2, one spheroid is formed at the bottom of each drop. Once formed, spheroids were recovered and immersed in a collagen I gel[20]. For this, a rat tail collagen I (Gibco) solution 2 mg/ml in Dulbecco's modified Eagle medium (DMEM, Sigma-Aldrich) with 10% fetal bovine serum (Natocor) and antibiotic/antimycotic (Invitrogen) was prepared and placed on the wells of a six multi-well plate (0.5 ml/well). Ten spheroids were placed on the surface of each well. After half an hour of incubation at 37° C, collagen solution becomes a gel and spheroids get immersed in it. Spheroids begin to invade the surrounding gel a day after seeding. Photographs were taken daily with an inverted optical microscope (Olympus) for five days. Spheroid core and invasion areas were measured from photographs through the ImageJ software (http://imagej.nih.gov/ij). Experiments were repeated three independent times.

2.2 In silico model

The two-dimensional mathematical model represents an invading microtumour as a composition of two tumour cell populations with different phenotype and behaviour: proliferative core cells and invasive peripheral cells. The model initiates from a unique tumour cell and considers two stages: an initial benign stage with only proliferation and a later malignant stage where invasion is also included. The benign stage lasts until the spheroid reaches the population mean radius (r_{inv}) when collagen seeding takes place. The model can be described in cylindrical coordinates by a two-dimensional reaction-convection-diffusion equation[14]:

$$\frac{\partial C(r,\theta)}{\partial t} = P\,C(r,\theta)\left[1-\frac{C(r,\theta)}{C_{max}}\right] + \nabla\cdot\left[D(r,\theta)\,\vec{\nabla}C(r,\theta)\right] - V_r(\theta)\,\nabla_r\cdot C(r,\theta) + S\,\delta(r-r_{core}) \quad (1)$$

where $C(r,\theta)$ is the concentration of tumour cells ($cells/\mu m^2$), r the radius from the spheroid center ($\mu m, r_{min} \le r \le r_{max}$), θ the angle correspondent to the azimuthal coordinate ($0 \le \theta < 2\pi$), t the time (h), P the net cell proliferation index ($cells/h$), C_{max} the maximum cell concentration (carrying capacity, $cells/\mu m^2$), $D(r,\theta)$ the cell diffusion coefficient ($\mu m^2/h$), $V_r(\theta)$ the radial cell velocity ($\mu m/h$, the angular component is negligible for the model), S the cell source ($cells/\mu m^2\ h$), $\delta(r-r_{core})$ the Dirac's delta function and r_{core} the spheroid core radius (μm). This δ function locates the cell source at the spheroid surface (r_{core}). The r_{core} is time-dependent and defines at each time point the limit between the spheroid core area ($0.0019\ cells/\mu m^2 \le C(r,\theta) \le C_{max}$) and the invasion area ($0 \le C(r,\theta) < 0.0019\ cells/\mu m^2$).

The first term represents the net cell proliferation (logistic law). The second term is a diffusive term based on the Fick's law that achieves both the volumetric growth of the spheroid as well as a non-directional component of the tumour invasion. The third term represents a radial convective component of the tumour invasion. Finally, the fourth term considers a source of tumour cells located at the spheroid surface. The final expression of equation 1 is:

$$\frac{\partial C(r,\theta)}{\partial t} = P\,C(r,\theta)\left[1-\frac{C(r,\theta)}{C_{max}}\right] + \frac{1}{r}\frac{\partial}{\partial r}\left[r\,D(r,\theta)\frac{\partial C(r,\theta)}{\partial r}\right] + \frac{1}{r^2}\frac{\partial}{\partial \theta}\left[D(r,\theta)\frac{\partial C(r,\theta)}{\partial \theta}\right] - \frac{V_r(\theta)}{r}\frac{\partial (r\,C(r,\theta))}{\partial r} + S\,\delta(r-r_{core}) \quad (2)$$

The boundary condition at $r = r_{max}$ is $\frac{\partial C}{\partial r}(r_{max},\theta) = 0$. Initial condition at t = 0 is $C(r,\theta) = 0$. The model was solved in a two-dimensional domain by finite differences with standard relaxation techniques and coded in Fortran 95. Main parameter values are presented in table 1. Following Stein at al.[14], we set at first P, D and V_r as constants depending only on the type of cell (P_{core} and D_{core} for core cells, P_{inv} and D_{inv} for invasive cells, V_r has no null values only for invasive cells). This initial approach provided an approximation to experimental invasion areas with spherical symmetry. For a more realistic description of invasion shapes,

we made in a second instance D_{inv} and V_r spatially variable. At this point the model may be used in two different ways: in a descriptive or a predictive manner.

Table 1 *In silico* model parameters

Parameter	Value	Parameter	Value
C_{max}	0.002 $cells/\mu m^2$	r_{inv}	70 μm
r_{min}	5 μm	r_{max}	855 μm
P_{core}	0.035 $cells/h$	P_{inv}	0.03 $cells/h$
D_{core}	0.5 $\mu m^2/h$	D_{inv}	36 $\mu m^2/h$
V_r	5 $\mu m/h$	S	$1.66e^{-8}$ $cells/\mu m^2 h$

Descriptive simulations: Descriptive simulations are case-specific as they reproduce the growth and invasion shape of a given experimental tumour case. We first generated a shape function by image processing that described the invasion area contour of a particular spheroid. This function assigned weight across the polar angle of the spheroid in the 360° domain based on the distance from the contour to the spheroid center. Then we normalized the curve of the invasion shape, discretized the angle coordinate and calculated at each point the correspondent invasion distance. This image processing was performed by a C++ code written for this purpose. Finally the shape function generated was used to feed the main model to make D_{inv} and V_r spatially variable and reproduce each experimental case. The whole process to make descriptive simulations is shown in figure 1.

Predictive simulations: Predictive simulations are population-dependent as they are generated aleatory based on the information taken from our entire database of tumours. For this, the whole database of shape functions obtained from our experimental images (more than 30 cases) were used to feed an EGARCH model (exponential, generalized, autoregressive, conditional heteroscedasticity model) taken from a Matlab toolbox (http://www.mathworks.com/help/econ/egarch-model.html). The EGARCH model, originated in the econometrix area for volatility clustering, makes a conditional variance temporal series analysis of each shape function and extracts a deterministic and a random component from the whole dataset. With this statistics, the toolbox forecasts, by Monte Carlo simulations, new aleatory shape functions that respond to the general population pattern. Finally, an aleatory-generated shape function was used to feed the main model to make D_{inv} and V_r spatially variable and predict a new possible tumour case. This approach lets a continuum feedback as new experimental data can be added at any time to the EGARCH model to improve population statistics.

Then the theoretical package may be used in two ways. We can feed the main model with a particular shape function to reproduce the growth and invasion of a microtumour in a case-specific way (descriptive simulations) or we can feed the model with an aleatory shape function elicited by the EGARCH model to generate new possible tumour cases that respond to the population pattern of this kind of tumour in these specific medium conditions (predictive simulations). In all cases Paraview was used for image visualization (http://www.paraview.org/).

3 Results and Discussion

Examples of the first use of the package (descriptive use) are presented in figure 2. Here we compare experimental spheroid images with simulated ones after five days of invasion. Experimental images show collective invasion into the collagen matrix, with epithelial cells organized into a laminar pattern. Two main patterns of cancer cell invasion have been described so far: collective and individual invasion. Among them, each specific pattern depends on the tumour cell type but also on the tumour microenvironment and stroma organization[21,22]. Human cancer pathology usually shows tumour cells invading collectively as strands, cords or clusters. On the other hand, experimental studies display from single isolated cells with round or elongated phenotypes (ameboid and fibroblast-like shapes, respectively) to loosely streams of cells or collective migration of cell strands or sheets.

Simulated core sizes of figure 2 were fitted to population data, while experimental invasion shapes are well reproduced in a case-specific way by their correspondent simulations. Table 2 presents invasion areas of both experimental and simulated images, the percentage difference between them (calculated in relation to total invasion area) and its average. Averaged difference between both areas are 17.15 %. Then simulations reproduce both qualitatively and quantitatively the experimental cases.

Table 2 Experimental and simulated invasion areas (μm^2) with their percentage differences correspondent to the cases of figure 2

Case	Experimental	Simulated	Difference (%)
1	0.259	0.211	18.85
2	0.068	0.088	22.75
3	0.194	0.201	3.76
4	0.117	0.188	37.74
5	0.205	0.206	0.12
6	0.200	0.166	16.95
7	0.283	0.253	10.86
8	0.066	0.097	32.15
9	0.151	0.163	7.55
10	0.260	0.206	20.79
Average			17.15
Stand. dev.			12.46

Examples of the second (predictive) use are presented in figure 3. Here we generate new possible and aleatory tumour cases at day five of invasion that respond to the general population pattern. Figure 4 shows a comparison between experimental and simulated main shape function statistics (mean, median and standard deviation) by the Bland & Altman method[23,24]. This method gives a good idea of the correspondence degree between model predictions and experimental data. For this purpose, a new different simulated shape function (generated aleatory by the EGARCH model) was produced to be compared with a given experimental one (extracted from a tumour case by image processing). It can be observed that, for the three statistics analyzed, regression intercepts and slopes are not significant (significance level at 0.05). This means that there are no significant differences between invasion patterns obtained from theoretical and experimental methods, and that differences are aleatory, not dependent on the mean between both methods. Then the mathematical model is reliable. This lets our experimental/numerical approach to be established

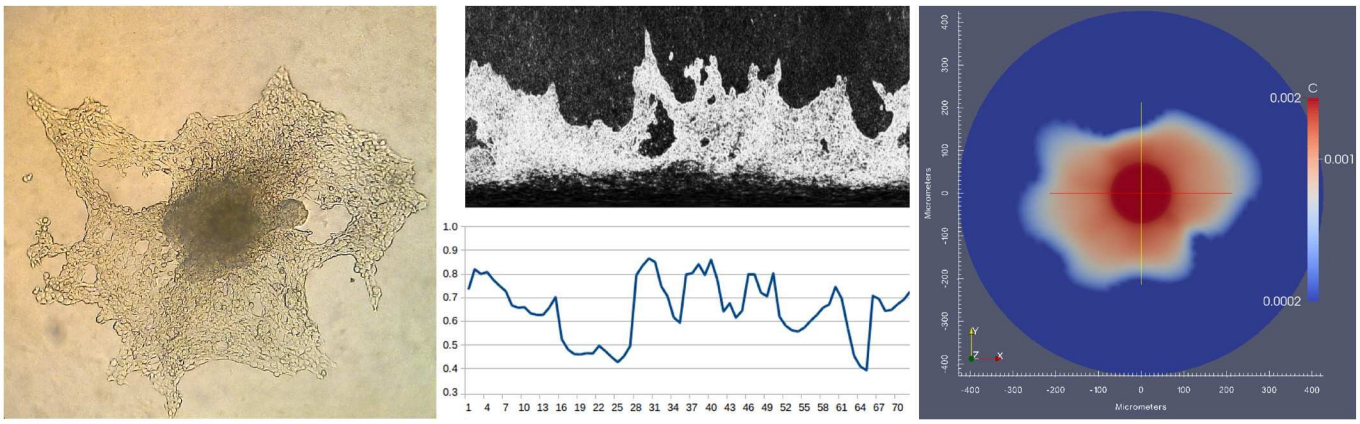

Fig. 1 Image processing – A) Initial experimental image of a multicellular tumour spheroid invading a collagen matrix (100x). The central tumour core can be well differentiated from the peripheral invasion area. B) Image binarization and transformation from Cartesian coordinates to polar coordinates. C) Generation of the shape function (invasion distance vs. polar coordinate). D) Final descriptive simulation that incorporates data from the shape function.

as a combined method to study different possible invasion patterns that may result from different tumour types and microenvironmental conditions.

Infiltration issues are specially critical in the case of gliomas. Gliomas are a disparate group of primary brain tumours that share the ability of penetrating diffusely throughout the brain, though they rarely metastasize outside the central nervous system. High-grade gliomas are a real challenge for present day oncology as, despite all modern therapies, they have very high morbidity and mortality[25]. It is proposed that this may be due, at least in part, to the fact that the real infiltration zone of these tumours is often non-spherical and underestimated when surgery or radiotherapy is applied[6]. Infiltration levels and its spatial organization depend both on the tumour type and stage as well as on the medium characteristics the tumour encounters when spreading. So this kind of tumours require a multidisciplinary and individually-adjusted treatment approach.

The in vitro model of multicellular tumour spheroids, combined with the correspondent mathematical modelling, has many experimental as well as clinical interesting potential applications for these kind of tumours. Firstly, this approach may be used to study the influence of bio-physicochemical characteristics of the extracellular medium on the invasion pattern of a tumour[16]. Secondly, it may be also used to test invasion properties and therapeutic responses of a given tumour when the spheroids are constructed in base on tumour cells derived from human biopsies[26,27]. At this stage, this theoretical/experimental framework may surely be an useful complementary clinical tool to help in tumour prognosis and treatment definition.

4 Conclusions

Mathematical modelling approaches have become increasingly abundant in cancer research. To shift the therapeutic paradigm towards a personalized care, precision medicine in oncology requires new powerful and interdisciplinary resources. In general, mathematical models of avascular microtumours have centered in the description of the volumetric growth of the spheroid and of rather spherical tumour invasion areas. Nevertheless real invasion areas are often not spherical and it is necessary the development of new strategies to better determine them. This, in many cases, is essential to achieve a clinical oncology translation useful to tumour prognosis and optimization of surgery or radiotherapy. Here we presented a two-dimensional mathematical model able to recreate the growth and real invasion shapes correspondent to a collective, laminar and epithelial pattern in a case-specific manner, as well as to predict new possible tumour cases in a population- and microenvironmental-dependent manner. This kind of experimental-numerical interaction has wide application potential at the moment of designing new strategies able to predict as much as possible the invasive behaviour and therapeutic response of a tumour in base on its particular characteristics and the bio-physicochemical medium conditions.

5 Acknowledgements

E. Luján has a fellowship from the Consejo Nacional de Investigaciones Científicas y Técnicas (CONICET). N. Visacovsky has a fellowship from the Instituto Nacional del Cancer (INC). L.N. Guerra, A. Soba, J.C. Calvo and C. Suárez are researchers at CONICET. We thank to Dr. Guillermo Marshall for his contributions to the manuscript, to Lic. David González Márquez for the development of the C++ code for image processing and to the Computational Simulation Center (CSC) from CONICET for the use of the cluster TUPAC for some of the simulations presented here. This work was supported by grants from CONICET (PIP GI 11220110100379) and Universidad de Buenos Aires (UBACyT GC 20620130100027BA).

References

1 L. Preziosi, *Cancer Modelling and Simulation*, Chapman & Hall/CRC, 2003.

2 D. Barbolosi, J. Ciccolini, B. Lacarelle, F. Barlési and N. André, *Nature Reviews Clinical Oncology*, 2016, **13**, 242–254.

3 P. Altrock, L. Liu and F. Michor, *Nature Reviews Cancer*, 2015, **15**, 730–745.

4 G. Powathil, M. Swat and M. Chaplain, *Seminars in Cancer Biology*, 2015, **30**, 13–20.

5 P. Jackson, J. Juliano, A. Hawkins-Daarud, R. Rockne and K. Swanson, *Bull Math Biol*, 2015, **77**, 846–856.

6 C. Suárez, F. Maglietti, M. Colonna, K. Breitburd and G. Marshall, *PlosOne*, 2012, **7**, e39616.

7 D. Loessner, J. Little, G. Pettet and D. Hutmacher, *Journal of Cell Science*, 2013, **126**, 2761–2771.

8 C. Wang, Z. Tang, Y. Zhao, R. Yao, L. Li and W. Sun, *Biofabrication*, 2014, **6**, 022001.

9 G. Benton, G. DeGray, H. Kleinman, J. George and I. Arnaoutova, *Plos One*, 2015, **10**, e0123312.

10 L. Weiswald, D. Bellet and V. Dangles-Marie, *Neoplasia*, 2015, **17**, 1–15.

11 A. Guzman, M. Ziperstein and L. Kaufman, *Biomaterials*, 2014, **35**, 6954–6963.

12 B. Hegedus, F. Marga, K. Jakab, K. Sharpe-Timms and G. Forgacs, *Biophysical Journal*, 2006, **91**, 2708–2716.

13 D. Loessner, J. Flegg, H. Byrne, J. Clements and D. Hutmacher, *Integrative Biology*, 2013, **5**, 597–605.

14 A. Stein, T. Demuth, D. Mobley, M. Berens and L. Sander, *Biophysical Journal*, 2007, **92**, 356–365.

15 A. Stein, M. Nowicki, T. Demuth, M. Berens, S. Lawler, E. Chiocca and L. Sander, *Appl Opt*, 2007, **46**, 5110–5118.

16 A. Anderson, A. Weaver, P. Cummings and V. Quaranta, *Cell*, 2006, **127**, 905–915.

17 V. Andasari, R. Roper, M. Swat and M. Chaplain, *Plos One*, 2012, **7**, e33726.

18 A. Urtreger, V. Ladeda, L. Puricelli, A. Rivelli, M. Vidal, E. Sacerdote de Lustig and E. Bal de Kier Joffé, *International Journal of Oncology*, 1997, **11**, 489–496.

19 J. Kelm, N. Timmins, C. Brown, M. Fussenegger and L. Nielsen, *Biotechnological Bioengineering*, 2003, **83**, 173–180.

20 L. Kaufman, C. Brangwynne, K. Kasza, E. Filippidi, V. Gordon, T. Deisboeck and D. Weitz, *Biophysical Journal*, 2005, **89**, 635–650.

21 N. Krakhmal, M. Zavyalova, E. Denisov, S. Vtorushin and V. Perelmuter, *Acta Naturae*, 2015, **7**, 17–28.

22 A. Clark and D. Vignjevic, *Current Opinions in Cellular Biology*, 2015, **36**, 13–22.

23 J. Bland and D. Altman, *Lancet*, 1986, **1**, 307–310.

24 J. Bland and D. Altman, *Ultrasound in Obstetrics & Gynecology*, 2003, **22**, 85–93.

25 T. Mesti and J. Ocvirk, *Radiol Oncol*, 2016, **50**, 129–138.

26 L. Ridder, M. Cornelissen and D. Ridder, *Critical Reviews in Oncology and Hematology*, 2000, **36**, 107–122.

27 K. Kross, J. Heimdal, C. Olsnes, J. Olofsson and H. Aarstad, *Scandinavian Journal of Immunology*, 2008, **67**, 392–399.

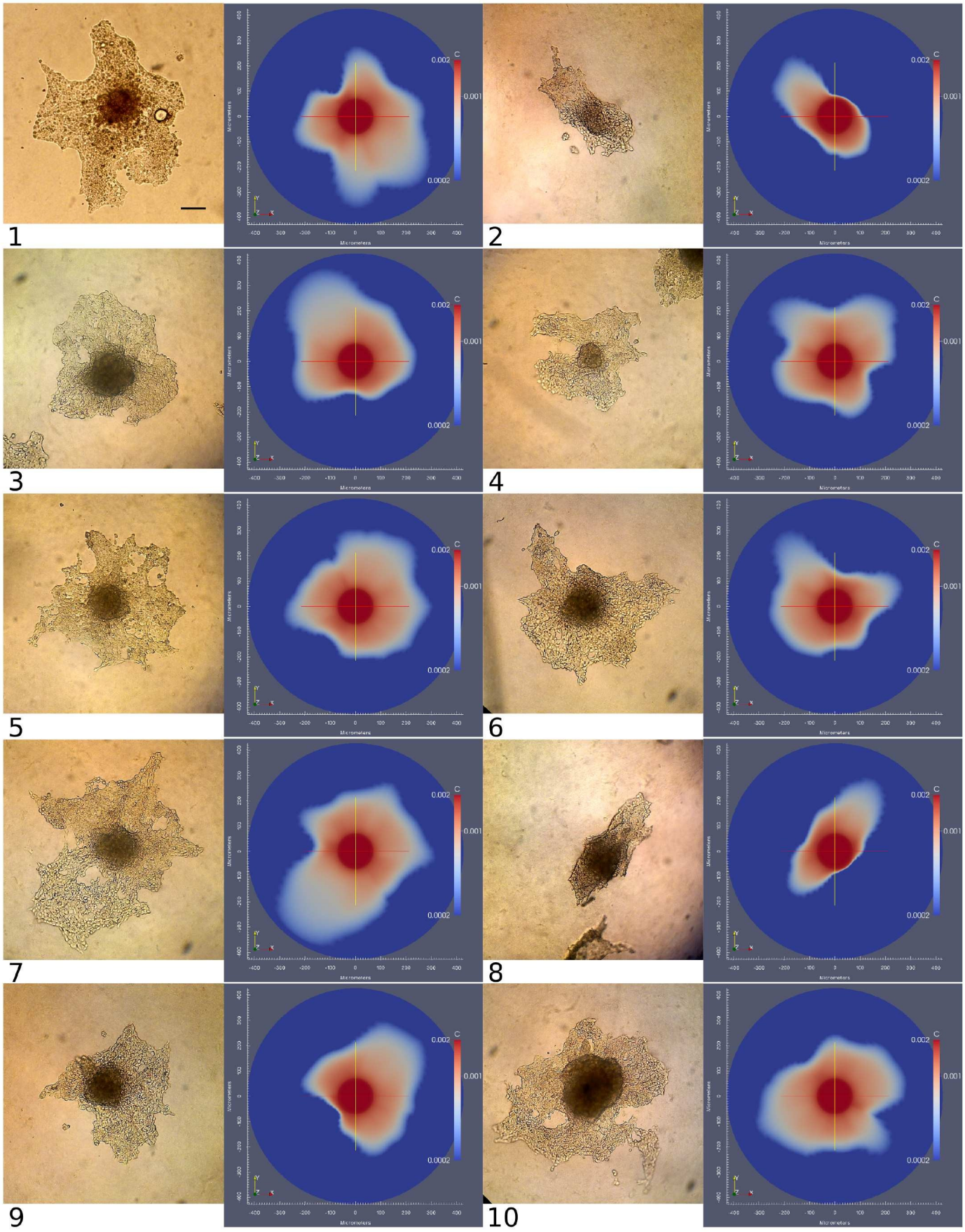

Fig. 2 Descriptive simulations (10 example cases) – First and third columns: experimental images of multicellular tumour spheroids invading a collagen matrix at the 5th day of invasion (100x). Scale bar represents 100 μm. Second and fourth columns: descriptive simulations of each individual experimental image, also at the 5th day of invasion. Spheroid core and invasion limits were set at 0.0019 and 0.0002 $cells/\mu m^2$, respectively.

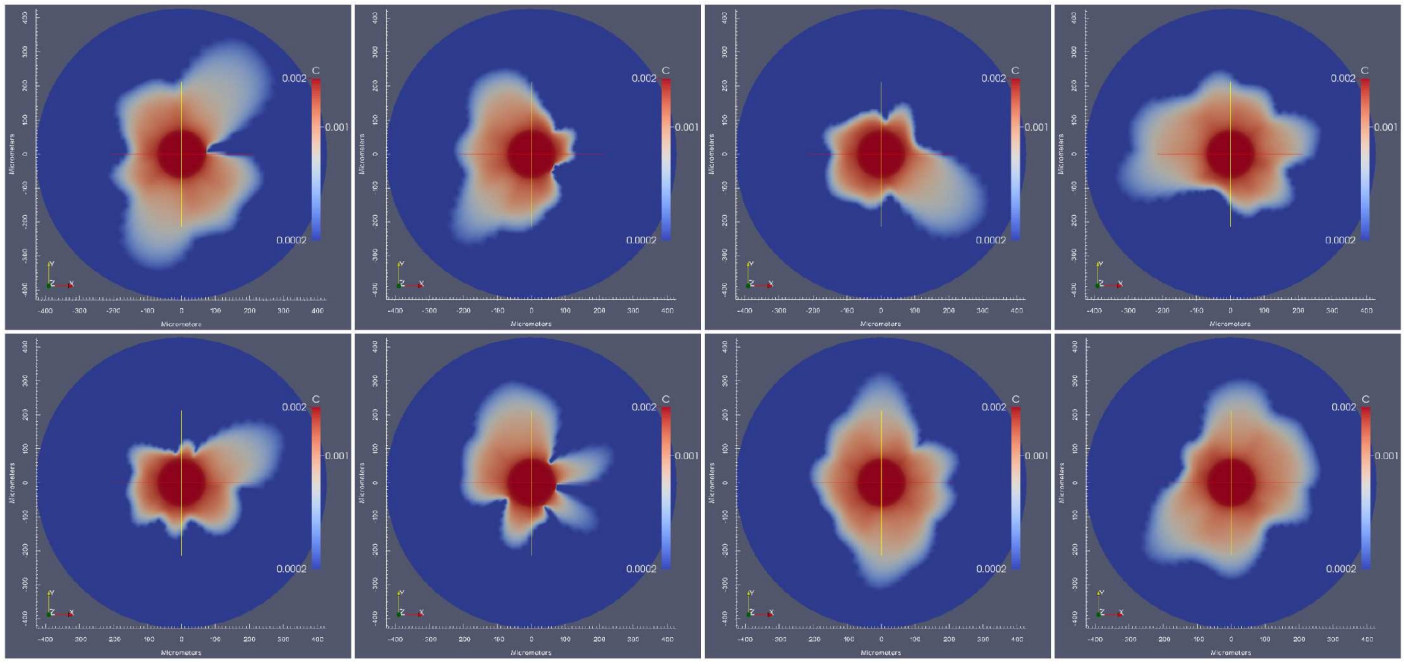

Fig. 3 Predictive simulations – Different simulations of multicellular tumour spheroids at day 5 of invasion in a collagen matrix generated aleatory by the model. Spheroid core and invasion limits were set at 0.0019 and 0.0002 $cells/\mu m^2$, respectively.

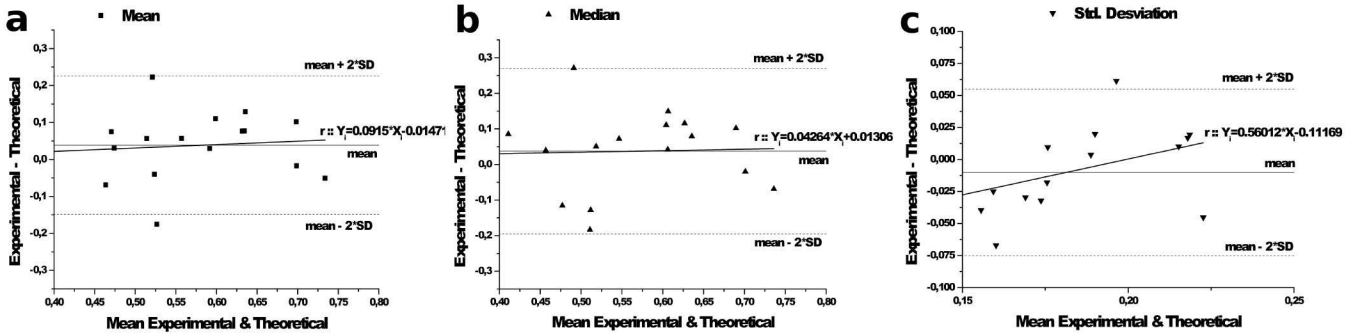

Fig. 4 Bland-Altman analysis of differences between experimental and theoretical main shape function statistics – A) Mean. Intercept: -0.0147 (p=0.932), slope: 0.0915 (p=0.755). B) Median. Intercept: 0.0131 (p=0.946), slope: 0.0426 (p=0.899). C) Standard deviation. Intercept: -0.112 (p=0.0458), slope: 0.56 (p=0.0638).

Table of contents entry

Mathematical modelling of microtumour infiltration based on in vitro experiments

Emmanuel Luján, Liliana N. Guerra, Alejandro Soba, Nicolás Visacovsky, Daniel Gandía, Juan C. Calvo, Cecilia Suárez

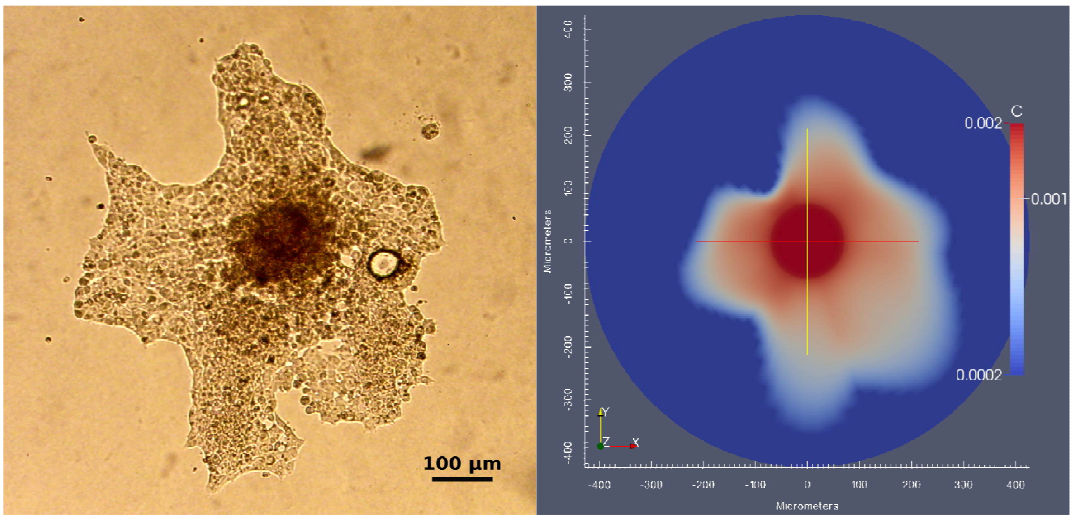

Numerical simulation of microtumor growth and infiltration in a collagen matrix based on case-specific or aleatory-generated shape functions.